Design of isolated buildings to achieve targeted collapse limits through Gaussian process modeling

Huy G. Pham[a], Tracy C. Becker, Ph.D., A.M ASCE[b,*]

[a] *University of California, Berkeley, Department of Civil & Environmental Engineering, Berkeley, 94720, California, USA*
[b] *University of California, Berkeley, Department of Civil & Environmental Engineering, 781 Davis Hall, Berkeley, 94720, California, USA*

Abstract

For conventional buildings, design codes are written such that minimally compliant buildings should achieve code-defined collapse probabilities under maximum considered events (MCE); however, there is no systematic methodology to ensure this is true for isolated buildings. Iterative design in which a building is designed, its collapse probability is assessed via incremental dynamic analysis (IDA), and the design is adjusted is inefficient given the number of permutations in the building-isolation system design. In an effort to find acceptable design parameters to achieve desired levels of collapse in early stages, full non-linear dynamic analysis can be bypassed through the use of data-driven predictive modeling. Gaussian process (GP) regression is utilized to fit and predict isolated building performance based on a generalized database. A sequential adaptive design of experiment (DoE) method is then used to strategically select training points to minimize the predictive variance of the GP model, and the model is then used to predict collapse probabilities for isolated structures. From here, designs that admit higher collapse probabilities than the threshold are removed, and cost optimization is performed to inversely select designs parameters such that the building will meet the targeted collapse probability under the MCE. Using this information, discussion on necessary required design parameters (e.g., moat clearance and strength reduction ratio) is given.

Keywords: seismic isolation, inverse design, Gaussian process, collapse probability, performance-based design

*Corresponding author
Email address: tcbecker@berkeley.edu (Tracy C. Becker, Ph.D., A.M ASCE)

1. Introduction

In recent years, significant effort has been made to advance performance-based seismic design for new construction of isolated structures[1, 2, 3]. Increasingly, structures of large importance and scale, such as hospitals, high rises, and other buildings that serve critical roles, are designed to performance-based metrics and seek to limit the casualties, cost of repair, and economic downtime in the case of a major seismic event. ASCE 7 [4] outlines targeted probabilities of failure under the risk-targeted maximum considered event (MCE_R) for buildings of various risk categories, and, through capacity design, conventional non-isolated structures typically achieve these targets. However, studies such as Bao and Becker [5], Shao and Mahin [6], and Kitayama and Constantinou [7] have shown that isolated structures designed to the ASCE 7-22 minimum criteria in Chapter 17 may have unacceptable collapse probability for the MCE_R. Although many designers choose to use more enhanced analysis in design such as nonlinear dynamic analysis, these studies have found that when prescriptively using the minimum design provisions, the isolator design displacements specified in the code may not satisfy targeted reliability for some seismically isolated structures.

However, the scopes of these studies are limited to a handful of archetype designs, and work remains to be done in generalizing the results to all permutations of isolated structures. Furthermore, the research generally observes the effect of only one or two design parameters at a time, such as the moat wall distance [8] or superstructure type and strength [5]. As a result, there is a lack of information from which regressions can be made and more generalized design parameters can be targeted based on the desired performance. Given the increased costs of design and construction for isolated buildings and the recent push for performance-based design, owners and designers should be able to easily target decreased collapse probabilities for the design of any generalized isolated structure based on a series of starting parameters characterizing the entire system.

As such, the goal for this study is to build a predictive model based on a generalized random database that allows a user to select the optimal design parameters given a targeted risk-specific objective. A full design space of parameters is included, characterizing both the properties of the isolation system as well as the main superstructure in relation to the hazard. A Gaussian process model serves as the predictive model from which a design can be optimized in conjunction with an appropriate user-defined cost function. Similar approaches to inverse design have been

utilized in previous research, such as Ning and Xie [9], using logistic regression to find optimal isolator and damping properties in bridge models, though optimized for minimizing annual repair cost rather than collapse probability. While the framework of this framework of the model can be adapted to any class of structures, the focus of the paper will demonstrate the process as applied to a steel moment frame isolated with triple friction pendulums (TFP) targeting a specific collapse probability.

Naturally, an exhaustive database that indexes all possible combinations of parameters and design is computationally expensive. As such, researchers have employed machine learning approaches to tackle the problem of modeling the design space probabilistically and optimizing a design based on the desired performance. The predictive model bypasses the need for high fidelity numerical modeling once the probabilistic model is built on an initial dataset. Gaussian processes (GPs), or kriging methods, is a machine learning approach often used in the engineering context due to its ability to incorporate known patterns into the representation of stochastic models. Previous studies have successfully applied GPs to enhance ground motion models [10] and lifecycle analyses [11]. These studies also incorporate adaptive design of experiments (DoE) to intelligently generate new design data to further reduce uncertainty in the models. For design, past studies using data-driven modeling, such as GP-aided design of floor isolation systems [12] or GP-aided design of high-rises under wind loading [13, 14], are focused on the design of a specific structure, rather than generalized (location independent) structural design parameters. Here, the GP-aided design is extended to both the superstructure and the isolation system through the generation of hazard level-normalized design parameters.

2. Methodology

Initially, a database of basis points is generated from which the predictive model is built with each basis point being the result of a single nonlinear dynamic analysis of a randomly designed moment frame coupled with a randomly selected ground motion run in OpenSees [15] and evaluated for collapse. The structures considered are special steel moment resisting frame (SMRF), ranging from 3 to 8 stories and 3 to 8 bays, isolated with triple friction pendulum bearings. Using the results as a training set, a predictive model is created using Gaussian processes. From the predictive model, design regions with high predictive variance are identified as candidates for additional numerical experiments. To target future experiments to regions where points are

more informative, a weighted scale factor based on the leave-one-out cross validation error of the dataset is applied. The weighted predictive variance is then used as the selection criteria for additional experiments. Additional designs are then generated and analyzed to return a new training point, and the GP model is updated and evaluated to ensure that the model's predictive accuracy reaches convergence.

2.1. Building design and modeling

For each basis point, a set of inputs is randomly generated from which the building design is automated, and a ground motion is scaled. Latin hypercube sampling with uniform distribution is utilized to select design parameters to ensure a good representation of isolator bearings and superstructures, providing a strong basis for the Gaussian process model. The design parameters and their ranges are presented in Table 1. Parameter ranges are chosen to reflect typical values that might be seen in the design of an isolated structure. The range of design spectrum acceleration at period $T = 1$ sec, S_1, is chosen to reflect typical values found in coastal CA. The range for the amplification of the moat gap is chosen to investigate potential increases from the code recommended value that might be necessary. The strength reduction factor R_y is treated as a random variable to explore the effects of increasing the superstructure strength. With an upper bound value of $R_y = 2.25$, prior to impact against the moat wall, the structure is expected to experience a small amount of yielding, and for the lower bound of $R_y = 0.5$ the structure is expected to remain elastic until impact. ASCE 7-22 limits the R_y value for isolated structures to 3/8 of the R_y of the fixed base system, capped at 2.0. For steel SMRFs this results in a maximum value of R_y of 2.0, though, here, this is raised to investigate additional strength reduction. However, in practice many engineers use a R_y of 1.

The ranges of bearing parameters are chosen to match typical ranges seen in isolated structures. The TFP bearing design is derived from the unidirectional multi-stage behavior of TFP bearings [16], excluding hardening. For simplicity, this study examines bearings with the outer sliding surfaces sharing the same friction coefficient and radius of curvature. For each combination of T_M, Q, and k_1/k_2, an effective damping ratio ζ_M is determined. With the spectral acceleration S_1, effective period T_M, and effective damping ζ_M, ASCE 7-22 gives the expected displacement capacity D_M of the isolated system as

$$D_M = \frac{gS\,a_{T_M}T_M^2}{4\pi^2 B_M} = \frac{gS_1T_M}{4\pi^2 B_M} \tag{1}$$

Table 1: Design inputs from Latin hypercube sampling

Input	Description	Lower bound	Upper bound
S_1	Spectral acceleration at $T = 1$ s	0.8	1.3
T_M	Target effective bearing period	2.5 sec	5.0 sec
k_1/k_2	Ratio of bearing inner to outer slider stiffness	5.0	18.0
Q	Normalized bearing backstrength	0.05	0.12
A_δ	Amplification for moat gap	0.5	1.2
R_y	Strength reduction factor	0.5	2.25
L_{bldg}	Length of building	23 m (75 ft)	76 m (250 ft)
h_{bldg}	Height of building	9 m (30 ft)	30 m (100 ft)

where B_M is the damping coefficient from ASCE 7-22, associated with the damping ratio ζ_M. The first sliding coefficient, μ_1, is specified by the designer, and the remainder of the bearing parameters are calculated as shown in Fenz and Constantinou [16] or Becker and Mahin [17]. D_M is not amplified for torsion as the analysis is conducted with a unidirectional ground motion. However, the constructed moat gap D_{moat} is modified by multiplying D_M by A_δ to explore its effect on the collapse probability.

The superstructure is then designed following the equivalent static lateral force procedure outlined in ASCE 7-22. The design base shear for the structure is calculated as $V_b = D_M k_M / R_y$, where k_M is the effective stiffness of the bearings. ASCE 7-22 allows a maximum story drift of $\theta = 0.015$ at the MCE_R level for isolated buildings. The additional stiffness required for drift controls the member sizing and introduces overstrength into the structure. The beams are first selected by narrowing W-shapes down to those that have sufficient second moment of area I_x to meet the drift requirements and section modulus Z_x to meet the strength requirements. The lightest compact W-shapes are selected for the beams, and then the columns are selected to ensure a strong column weak beam mechanism. At the end of the design procedure, the friction coefficients μ, slider radii of curvature R, moat gap D_{moat}, column sections, and beam sections have been selected.

A 2-D model is constructed in OpenSees. The modeling details are provided in Figure 1. Beam and column elements are modeled using elastic beams with a bilinear rotational spring that exhibits strength deterioration at each end using the modified Ibarra-Krawinkler material

model. Parameters for the material model are selected for the beam sections chosen, placing each plastic hinge at 10% of the member length away from each joint [18]. A leaning column is incorporated to include the mass from the unmodeled gravity frames and to model P-Δ forces from the rest of the structure. A rigid diaphragm using elastic elements spans the layer above the isolators. The superstructure is assigned 5% stiffness proportional damping.

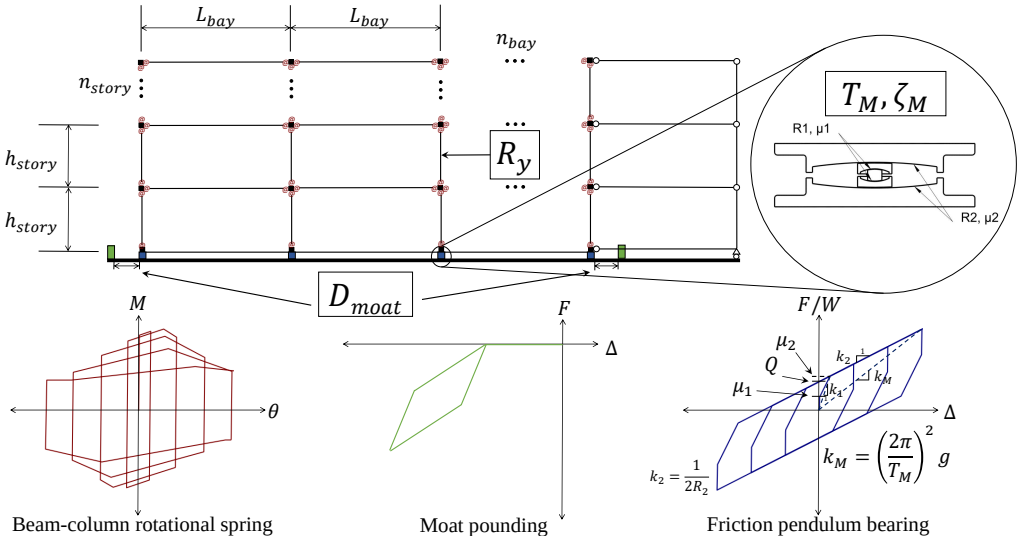

Figure 1: Modeling components of the TFP-isolated steel moment frames

The bearings are modeled with triple friction pendulum elements using simple Coulomb friction [19]. For this study, uplift is not considered as a failure mode due to the complexity of modeling the bearing uplift behavior. The moat wall is implemented using zero-length impact elements, which use an approximated damped Hertz contact model with calibration parameters as provided by Muthukumar and DesRoches [20].

For this study, collapse is judged by a collapse fragility curve, shown in Figure 2, using a lognormal cumulative distribution function. For the SMRF, the distribution is defined with 84% probability of collapse at a drift $\theta = 0.10$ and a dispersion of $\beta = 0.25$ for frames with less than 4 stories and a $\beta = 0.35$ for taller frames [21]. Sensitivity to this definition is later discussed, as structures such as intermediate or ordinary moment frames will damage and fail at lower drift ratios. As the displacement of the isolators are bound by the moat, their failure is not included in the analysis.

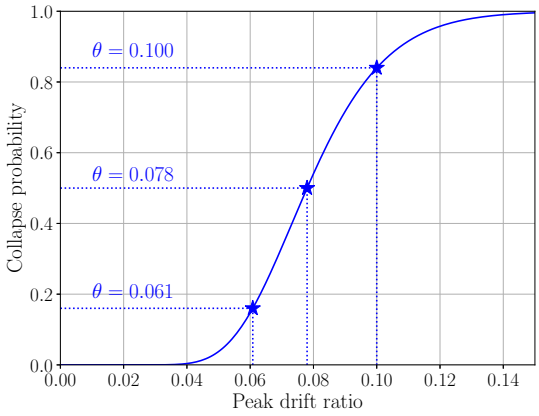

Figure 2: Defined collapse fragility curve for special steel moment resisting frame

2.2. *Ground motion scaling*

A library of 133 ground motion records is collected via the PEER NGA-West database [22] from events of magnitudes ranging from 6.0 to 8.0 and distances from 0.0 km to 80.0 km. $V_{s,30}$ velocities were limited from 200 m/s to 600 m/s to select for site with dense soil or soft rock. For each trial, a random S_1 is generated to create a target spectrum. A random ground motion is selected and then scaled over a range of interest, defined as $T = [0.2T_M, 1.5T_M]$ seconds. As this range does not extend into the constant acceleration region, the design spectrum is created without the need for an S_S value. The scaled ground motion's actual pseudo-acceleration at T_M, Sa_{T_M}, is recorded. This spectral acceleration is selected to represent the intensity measure as it appears in the ASCE 7-22 displacement capacity D_M.

2.3. *Generalized design parameters*

To generalize findings across a range of sites with different seismic hazard and different structural configurations, generalized design parameters are used for the inputs to the predictive model. Furthermore, using generalized parameters for the GP model has the advantage of generalizing the problem across different isolation systems without being constrained to friction pendulum bearings. For each design, the parameters are calculated after input variables are selected, and the isolated structure is designed. The dimensionless parameters are chosen due to their direct connection to the design.

A set of six design variables relevant to isolated system design (D_{moat}, T_M, T_{fb}, ζ_M, R_y, $S\,a_{T_M}$) is considered for this problem. The variables ζ_M, T_M/T_{fb}, and R_y represent the structural damping, effective isolation period amplification, and strength reduction factor, respectively. ζ_M, and R_y are already dimensionless, and T_M is normalized with T_{fb}, the calculated fundamental period of the equivalent fixed base superstructure, to characterize the isolation period lengthening. The remaining variables are reduced into the moat gap ratio $GR = 4\pi^2 D_{\text{moat}} \,/\, (S\,a_{T_M} g/B_M) T_M^2$. This parameter relates the constructed moat gap to the linear displacement demand from the hazard being designed for. For ASCE 7-22 compliance, the MCE_R would be considered. The list of covariates for the GP model is then finalized as GR, ζ_M, R_y, and T_M/T_{fb}.

2.4. Gaussian process model

To enable the selection of an inverse design, the probability of collapse across the design space needs to be estimated, which presents a major challenge in the inverse design problem. The calculation of collapse probability for every point in the design space would require a prohibitive amount of dynamic analyses performed. In lieu of this, Gaussian process [23] is used as a surrogate model to allow for efficient calculation of the probability of collapse $p(\mathbf{x})$ over the design space. The advantages of choosing a GP are multi-faceted. First, GPs are analytic in nature, meaning that the optimized model is computed exactly in closed form. This, in turn, allows for the direct calculation of the regressed mean predictions and bias metrics such as the leave-one-out error. GPs are also generative models, which means that a probability distribution is determined for each prediction involving both the mean and variance, which allows for design-of-experiment procedures to be carried out targeting high variance regions, as well as probabilistic outcomes, such as collapse probability, to be inferred. Additionally, the choice of covariance functions, or kernels, in specifying the GP allows for prior knowledge to be applied to the regression.

The Gaussian process (Equation 2) is defined by a mean function $\mu(\mathbf{x})$, which expresses the prior expected output of the input and a covariance function $k(\mathbf{x}, \mathbf{x}')$ which expresses the similarity of inputs in their effects on the output and provides a representation of the features of $\mathbf{x}$ to train upon. The underlying function is then expressed as

$$f(\mathbf{x}) = GP\left(\mu(\mathbf{x}), k(\mathbf{x}, \mathbf{x}')\right) \tag{2}$$

The outcome of collapse probability y is the Gaussian process combined with a noise variable ϵ.

$$y = f(\mathbf{x}) + \epsilon \tag{3}$$

Ultimately, the goal of Gaussian process regression is to predict the outcome, which in this study is the posterior probability that a new design point collapses. A prior mean function and covariance is then placed on the GP prediction $f(\mathbf{x})$. A zero-mean function $\mu(\mathbf{x}) = 0$ is chosen to avoid placing a prior relationship between design parameters and collapse probability. Therefore, expressions for the predictive mean and variance consist entirely of the GP's kernel components.

For the covariance function, the squared exponential kernel with an isotropic lengthscale (SE-ISO) augmented with white noise is chosen, in which one lengthscale is shared between all covariates. The SE-ISO kernel is defined as

$$k(\mathbf{x}, \mathbf{x}') = a \exp\left(-\frac{1}{2}\frac{\|\mathbf{x} - \mathbf{x}'\|^2}{\ell^2}\right) + \sigma_n^2 I\left[\mathbf{x} = \mathbf{x}'\right] \tag{4}$$

which requires the hyperparameters a, a scaling coefficient, the lengthscale parameter ℓ, and the white noise parameter σ_n^2 to determine the covariance between two points $\mathbf{x}$ and $\mathbf{x}'$. The white noise σ_n^2 is present if $\mathbf{x} = \mathbf{x}'$. The squared exponential kernel is commonly used in GP regression and is chosen here for its smoothness. The isotropic lengthscale ℓ is deliberately favored over a separate ℓ for each covariate. This results in variables with stronger correlations having a more "tempered" effect on the response, while variables with weaker correlations see their effects boosted. Previous trials of this study used individual lengthscales for each design variable by using the squared exponential kernel with automatic relevance determination. This resulted in overprediction based on GR while ignoring the effects of T_M/T_{fb}, which is later seen to be influential in Figure 4. Thus, the SE-ISO kernel is favored. This is chosen to explore interaction between all variables regardless of their importance and also to highlight more nuanced effects that bearing parameters might play on collapse probability.

The hyperparameters are free variables in the regression and are determined by optimizing the dataset's likelihood, whereby the log marginal likelihood of the training data is maximized using the Broyden-Fletcher-Goldfarb-Shanno algorithm [24]. Upon optimization of the hyperparameters, the GP model then returns a best fit predictive mean and variance of collapse probability for any given point $\mathbf{x}^*$ as closed form expressions by forming the posterior distribution, arriving at

$$f(\mathbf{x}^*) = k(\mathbf{x}, \mathbf{x}^*)^\top \left[k(\mathbf{x}, \mathbf{x}) + \sigma_n^2 I\right]^{-1} \mathbf{y} \tag{5}$$

where I is the identity matrix, f^* is the mean prediction of the unknown test point $\mathbf{x}^*$, and $\{\mathbf{x}, \mathbf{y}\}$ form the existing dataset.

2.5. Adaptive design of experiment

Although creating the initial database using a Latin hypercube with variables from Table 1 allows for a uniform distribution of input parameters in the design space, the database has shortcomings. First, there is no rigidly defined quantity of initial data points deemed "sufficient"; this is especially important for the problem of predicting structural collapse which is particularly noisy. Accordingly, there lacks a way to determine if the variance or accuracy metrics of the model's predictive capabilities have converged. Additionally, although the data uniformly covers the space of the input parameters, there is no guarantee that the output is equally informative across the space of the design parameters. For example, regions where the *GR* and superstructure strength are large result in consistent non-collapse predictions, meaning that the GP model does not gain information useful for reducing collapse prediction errors in regions where variance and collapse likelihood are high.

To address these shortcomings, an adaptive DoE is used to augment the GP model. This process seeks to selectively introduce new data points that maximize the information gain while running the fewest additional experiments as possible [25]. A DoE process based on reducing the predictive variance of the GP is utilized to introduce new experiments. Sequential design of experiment seeks to find an additional data point $\mathbf{x}_{n+1}$ that will increase the information gain, which is defined in this study as MSE_w, the localized mean squared error (MSE) at the candidate point evaluated under the current dataset weighted with the leave-one-out cross-validation (LOOCV) error [26] :

$$MSE_w(\mathbf{x}) = W(x)\,\sigma^2(\mathbf{x}|\mathbf{X}) \tag{6}$$

where $\sigma^2(\mathbf{x}|\mathbf{X})$ is the predictive variance of the GP at the current point $\mathbf{x}$ under the current dataset $\mathbf{X}$:

$$\sigma^2(\mathbf{x}|\mathbf{X}) = k(\mathbf{x}^*, \mathbf{x}^*) - k(\mathbf{x}, \mathbf{x}^*)^\top \left[k(\mathbf{x}, \mathbf{x}) + \sigma_n^2 I\right]^{-1} k(\mathbf{x}, \mathbf{x}^*) \tag{7}$$

$W(\mathbf{x})$ is a weight defined by

$$W(\mathbf{x}) = \frac{\sum_{i=1}^{n} \gamma(\mathbf{x}, \mathbf{x}_i) \left(e_i^{cv}\right)^2}{\sum_{i=1}^{n} \gamma(\mathbf{x}, \mathbf{x}_i)} \tag{8}$$

where e_i^{cv} is the LOOCV error associated with omitting point $\mathbf{x}_i$ from the GP. e_i^{cv} can be calculated in closed-form [27] upon tuning the GP at the current step and serves as a proxy to approximate

prediction bias and infer "important" regions in the model, and is expressed as

$$e_i^{cv} = \frac{\left[k(\mathbf{x},\mathbf{x})^{-1}\mathbf{y}\right]_i}{k(\mathbf{x},\mathbf{x})_{ii}^{-1}} \tag{9}$$

Since the value is only known at discrete values of the existing points $\mathbf{x}_i$ in the training set, a smoothing weight $\gamma(\mathbf{x},\mathbf{x}_i)$ inversely proportional to the normalized distance to point $\mathbf{x}_i$ is used to extrapolate e_i^{cv} to every point in the design space

$$\gamma(\mathbf{x},\mathbf{x}_i) = \exp\left(-\left\|\frac{\mathbf{x}-\mathbf{x}_i}{\ell}\right\|^2\right) \tag{10}$$

where $\|\cdot\|$ is chosen as a L^2-vector norm, ℓ is the lengthscale hyperparameter of the kernel in Equation 4, and the division in the function is element-wise.

The ideal point added by DoE is then a point $\mathbf{x}_{n+1}$ that maximizes $MSE_w(\mathbf{x})$; however, this criterion simply involves the estimation of the localized mean squared error without considering its impact on the mean squared error of the design space as a whole. This leads to several negative side effects, such as a tendency to place new experiments in boundary regions or clustered in the same location. Although this can be combated by using an integrated MSE approach, a proportional sampling approach is opted for in this study to save computational burden. The selection criterion MSE_w is evaluated across considered design space and is used as a desired sampling probability. During the design of experiments, additional experiment points are sampled proportionally to the selection criterion MSE_w using rejection sampling in batches of multiple points. By using proportional sampling to select batches of data points proportional to MSE_w, new points introduced are more likely to be in regions exhibiting both high variance and equal likelihood of having collapse as non-collapse, although points in regions of lower MSE_w are still occasionally added to provide additional exploration of points across the domain. This is particularly useful when the model lacks data to distinguish regions of distinctly high variance or bias (flatter distributions of MSE_w), such as the case when the DoE process is starting from a smaller dataset. In this study, the batch size is set at 5 experiments, and the GP model is refit after every batch to update the hyperparameters regularly while still using the advantages of batch sampling described above.

To assess the global accuracy of the GP model, this study uses a normalized root mean squared error (NRMSE) of the LOOCV error metric

$$NRMSE_{cv} = \frac{\sqrt{\sum_{i=1}^{n}\left(e_i^{cv}\right)^2/n}}{\max_i y_i - \min_i y_i} \tag{11}$$

where y_i are the outcome probabilities of collapse in the training set. This study uses two stopping criteria for the DoE process: a global accuracy metric defined as the reduction of $NRMSE_{cv}$ below a threshold of 0.01, or a relative convergence metric defined as when $NRMSE_{cv}$ does not change more than 0.001 for 10 added batches in a row. The motivation for the global accuracy metric is to attempt to achieve an average error of prediction roughly equal to 1% of collapse. The relative convergence metric is used to identify when the DoE model achieves diminishing return, and the selected 0.001 threshold, representing 0.1% difference in collapse probability prediction relative to its previous iteration, serves to limit the size of the training set to keep the $O(n^3)$ computational burden of the GP regression to a reasonable magnitude.

2.6. Grid search on cost function

After the completion of the DoE process, the final database is used to train the Gaussian process model, and the model returns collapse probability predictions for a uniform mesh over all possible design points. The inverse design problem can now be formulated as the optimization problem

$$\mathbf{x}^* = \arg\min_{\mathbf{x}\in\mathbf{X}_a} c(\mathbf{x}) \tag{12}$$

where $c(\mathbf{x})$ is the construction cost of the design $\mathbf{x}$, a function of the cost of erecting the frame as well as the land cost to accommodate the isolation gap. In the optimization problem above, the chosen design $\mathbf{x}^*$ is restricted to only designs in the subspace $\mathbf{X}_a$ of designs that satisfy the acceptable collapse probability limit

$$p(\mathbf{x}) \leq p^* \tag{13}$$

where p^* is the acceptable collapse probability limit at a given hazard level, and $p(\mathbf{x})$ is the GP-predicted collapse probability. The inverse design optimization problem in Equation 12 is solved by minimizing the cost function $c(\mathbf{x})$ via a simple grid search. In practice, commonly defined cost functions for optimization could be related to the cost of the structure, mean annual loss, losses under a specified intensity measure, or metrics pertaining to the physical performance of the structure, such as peak story acceleration or isolation layer displacement.

Here, a simple cost function is defined considering representative upfront construction and development costs of the steel in the superstructure and the land given the moat distance. The land cost is taken as \$2,837 per m^2 (\$263 per sq ft) as a representative value of development in San Francisco, CA [28]. To estimate the cost of the superstructure strength, a unit cost of \$4.41

per kg. ($2.00 per lb) is taken for steel. The cost of each structure in the database is calculated and normalized by the building area to account for varying building layouts. A linear regression is then performed for the normalized steel cost on the design base shear for the superstructure (V_s). The total cost function is then evaluated as

$$c(\mathbf{x}) = \$263 \times A_{\text{moat}}(\mathbf{x}) + (C_1 V_s(\mathbf{x}) + C_2) \times A_{\text{bldg}}(\mathbf{x}) \tag{14}$$

where A_{moat} and A_{bldg} are the areas covered by the building plus moat and just the building respectively, and C_1 and C_2 are regression coefficients for a structure's steel cost per area as a function of the design base shear. From the final database, the coefficients are $C_1 = 1.51 \times 10^{-3}$ and $C_2 = 13.7$. The cost function is then minimized over the acceptable design space using a grid search across combinations of design variables.

3. Example design selection

To illustrate the inverse design method, three cost-optimal designs are sought for isolated SMRFs, targeting 10%, 5%, and 2.5% maximum collapse probability.

3.1. Data trends and design of experiment

An initial data set of 50 trials was generated, and the completed DoE process resulted in a final database of 785 experiments. The convergence history of the root mean squared error on a test set (RMSE), the leave one out cross validation NRMSE, as well as the NRMSE's change are shown Figure 3. In addition to the initial 50 training points, 50 additional points were kept unseen from the GP model as a test set to benchmark the GP's accuracy. In this example, the global accuracy metric is never achieved, but rather the DoE process is halted by the relative convergence metric. The GP model initially sees improvement as points are added, and the RMSE on the test set converges to around 0.122. The NRMSE-LOOCV is measured on the training set as simulations are added during the DoE process, and the value hovers around a range of around 0.10 to 0.13 until the relative convergence criterion is reached. In Figure 3c), the change in NRMSE-LOOCV decreases with diminishing return after approximately 100 points added, which implies gradual convergence of NRMSE-LOOCV. There are abrupt changes in the NRMSE-LOOCV, which can be explained as the addition of data points that are more difficult to predict (e.g. higher collapse likelihood than predicted); however, the magnitude of changes

decrease as the set approaches convergence. Although a stricter convergence criterion could be defined, it is also prudent to avoid overfitting on the training set, demonstrated by the plateau in improvements to accuracy on the holdout set in Figure 3a).

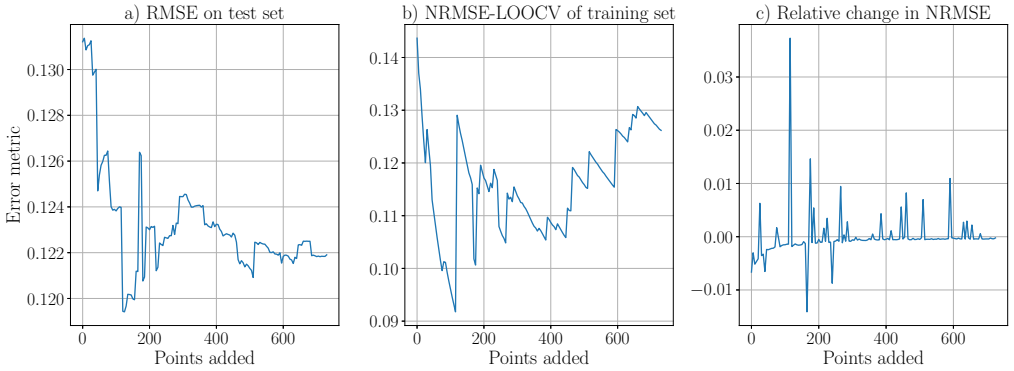

Figure 3: Convergence history of a) holdout set RMSE; b) LOOCV-NRMSE of the training set; and c) difference in NRMSE-LOOCV from the previous batch of points

Across all simulations, 31.2% experienced impact against the moat wall, and the mean peak drift across the dataset is $\theta = 0.019$. The distribution of the input parameters against the output peak drift of the structural analyses is shown in Figure 4, categorized by if the building impacts the moat wall. Generally, moat wall impact results in a distinct increase in recorded story drift. As such, there is a clear trend between the GR and drift. Weaker trends are present in R_y and T_M/T_{fb}, which sees slight correlation between lower drift and decreasing R_y or increasing T_M/T_{fb}.

Figure 5 shows the histogram of the original set of data, as well as the points added via DoE. Although the original dataset is generated with a uniform distribution of the inputs in Table 1, the original point histogram shows that this distribution is non-uniform in several dimensions of the design variables. After the DoE selections, several additional observations can be made regarding the choice of the points. The DoE strategy exhibits exploration characteristics, notably by adding points in low ζ_M and higher GR domains, where variance is high due to the sparsity of data in the original set. The DoE criterion also shows characteristics of bias exploitation by adding experiments where collapse is more likely, which is seen by a higher density of points added in higher R_y and lower T_M/T_{fb} regions. This shows that using proportional sampling to the weighted variance criterion results in new points in both regions of high variance and regions

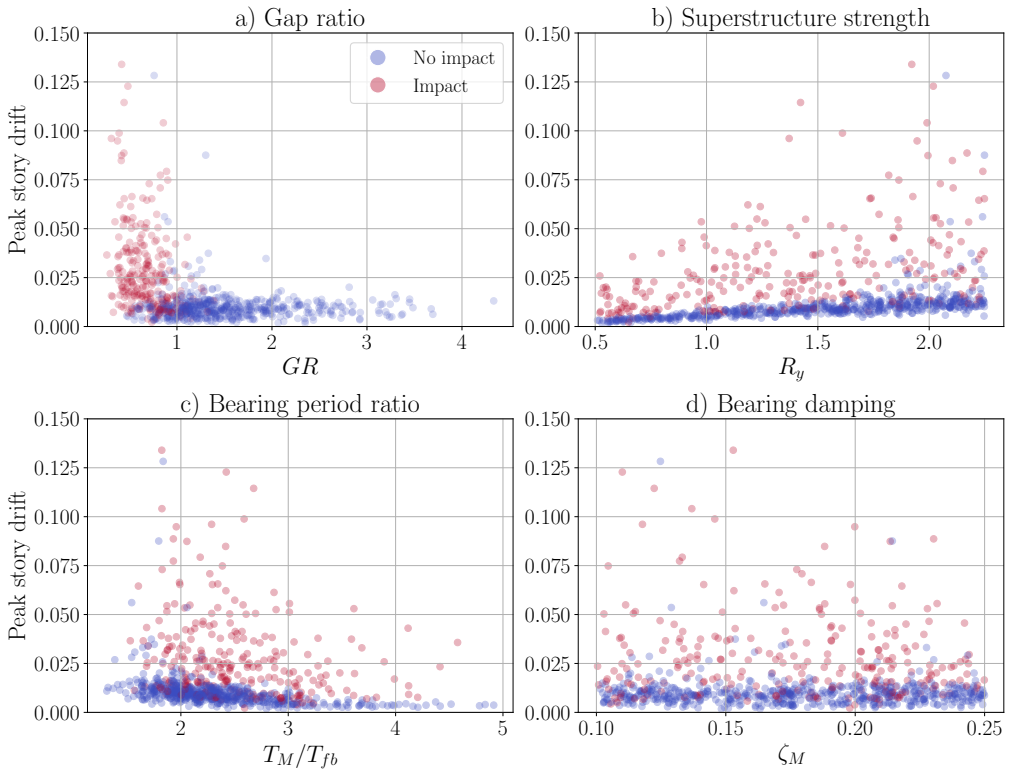

Figure 4: Effect of design variables on peak story drift

where individual data points contribute more to the overall prediction.

Figure 6 compares the GP predictions of collapse at 2D slices in the 4 design dimensions using the initial dataset and the finalized dataset with 735 additional points. Figure 6b) shows the MSE_w selection criterion. From the initial 50 points, very few of the displayed points in Figure 6a) exhibits significant collapse probability, and the collapse predictions are low across the design space. Figure 6b) shows that the selection criterion favors structures with low GR, with a preference for weaker structures (higher R_y). Figures 6c) and d) show the final model predictions. Compared to the pre-DoE model, Figure 6c) shows a higher collapse probability, particularly with the top left corner (weaker superstructures, smaller isolation gaps) having a sharp increase in collapse probability compared to the initial predictions. In the T_M/T_{fb} and ζ_M dimensions, shown in Figure 6d), predictions show a higher collapse probability for lower damping ratios and smaller T_M/T_{fb}.

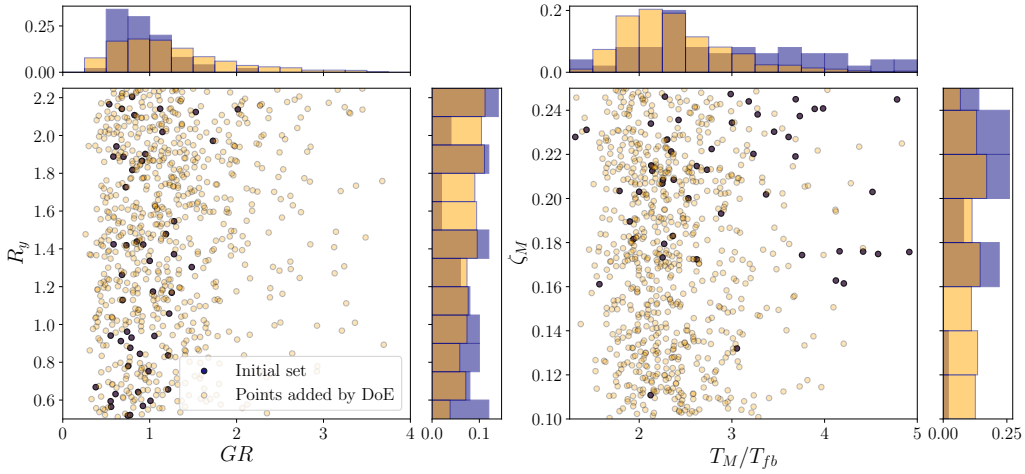

Figure 5: Comparison of distributions for original and post-DoE data sets

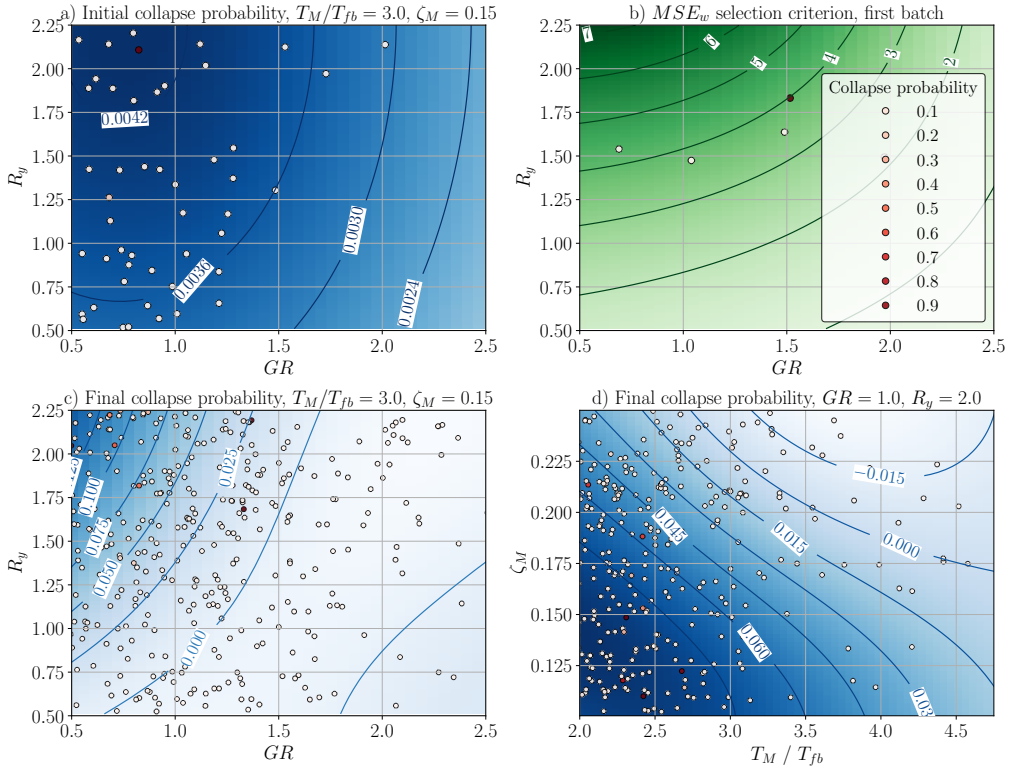

Figure 6: Illustration of GP predictions and DoE selection metrics of the DoE at several stages of the DoE process

3.2. GP model predictions

After supplementing the initial database with additional experiments, the GP model is evaluated. Figure 7 presents the contours of the predicted probability of collapse across a range of design parameters. The contours indicate that increasing *GR* and superstructure strength both heavily influences the collapse probability. Since impact against the moat wall introduces extremely large forces that result in drift, it is reasonable that larger moat gaps are the dominant contributors to decreasing collapse likelihood. Comparing the two columns of the figure, R_y is effective in reducing collapse probability, more so under smaller T_M/T_{fb} conditions, where the displacement responses are not strongly concentrated in the isolation layer. Under higher T_M/T_{fb} values, *GR* clearly has more influence than R_y. These results are consistent with the findings of Bao and Becker [5], which found that designs increasing displacement capacity reduces failure probability more than designing the frame to be stronger.

Figure 7 also shows the minimum gap necessary to achieve several collapse probability targets at $R_y = 2.0$. For a SMRF, to achieve 10% collapse with $T_M/T_{fb} = 2.0$, $\zeta_M = 0.15$, and $R_y = 2.0$ (Figure 7c), the GP model suggests that the gap ratio should be at 0.93, that is 93% of the code-specified expected maximum displacement. By lowering R_y to 1.5, thereby increasing superstructure strength by 25%, the required *GR* to maintain the same probability of collapse reduces dramatically, from 0.89 to 0.47. It is important to note that this study focuses on collapse and does not cover functionality of the building. Therefore, designs found to be sufficient in achieving the desired collapse may sustain significant damage, attaining high story drifts to magnitudes that would require significant repair if not complete replacement. It is expected that imposing higher functionality targets on the GP would push the design boundary for the parameters to be more conservative.

Figure 7 also shows the corresponding recommended *GR* for contours of lower collapse probabilities of 5% and 2.5%. At 5% target, the required *GR* in Figure 7c) is 1.27 (27% above code minimum) for $R_y = 2.0$. This gap amplification increases to 1.50 (50% larger than code minimum) when targeting 2.5% collapse probability. ASCE 7-22 does not provide for different designs for higher performance targets for isolated structures, however as shown, larger *GR* and stronger superstructures are recommended when aiming for lower collapse probabilities. Values for displacement limits given fixed R_y, T_M/T_{fb}, and ζ_M, as illustrated in Figure 7, could be used in codes to enable targeted performance.

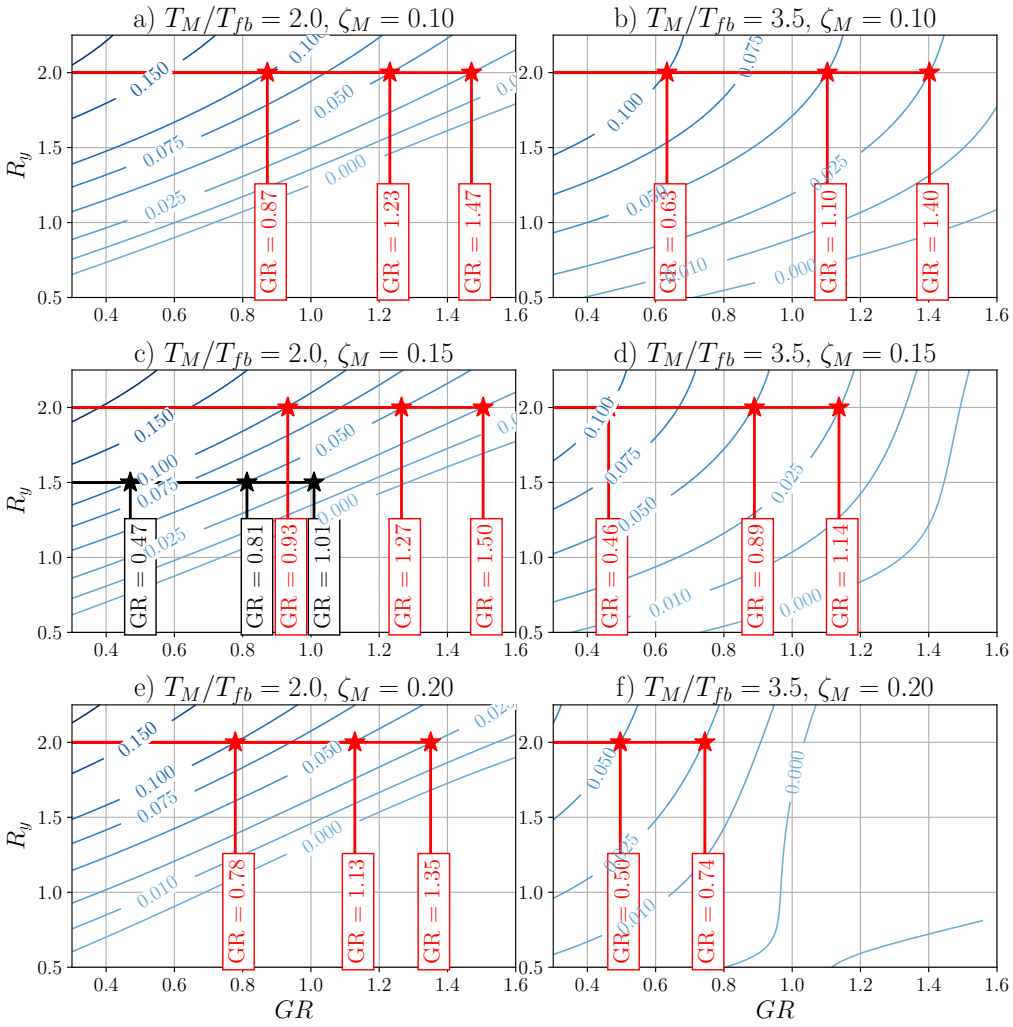

Figure 7: GP predicted collapse probability contours at several constant T_M/T_{fb} and ζ_M values. Constant lines show minimum allowable GR at fixed R_y for 10%, 5% and 2.5% risk targets from left to right

The effects of T_M/T_{fb} and ζ_M are visible across the plots in Figure 7 and are directly plotted in Figure 8. From the scatter plots in Figure 4, it should be expected that these variables have an effect on collapse probability, albeit less markedly compared to GR and R_y. Increasing T_M/T_{fb}, observed by moving from Figures 7a), c), and e) to the respective Figures 7b), d), and f), results in an overall reduction of collapse probability on the contours, allowing for smaller acceptable GR values to attain the same collapse probability. This agrees with the core concept of base

isolation, which favors higher period amplification of the structure to lower the spectral demands felt on the system.

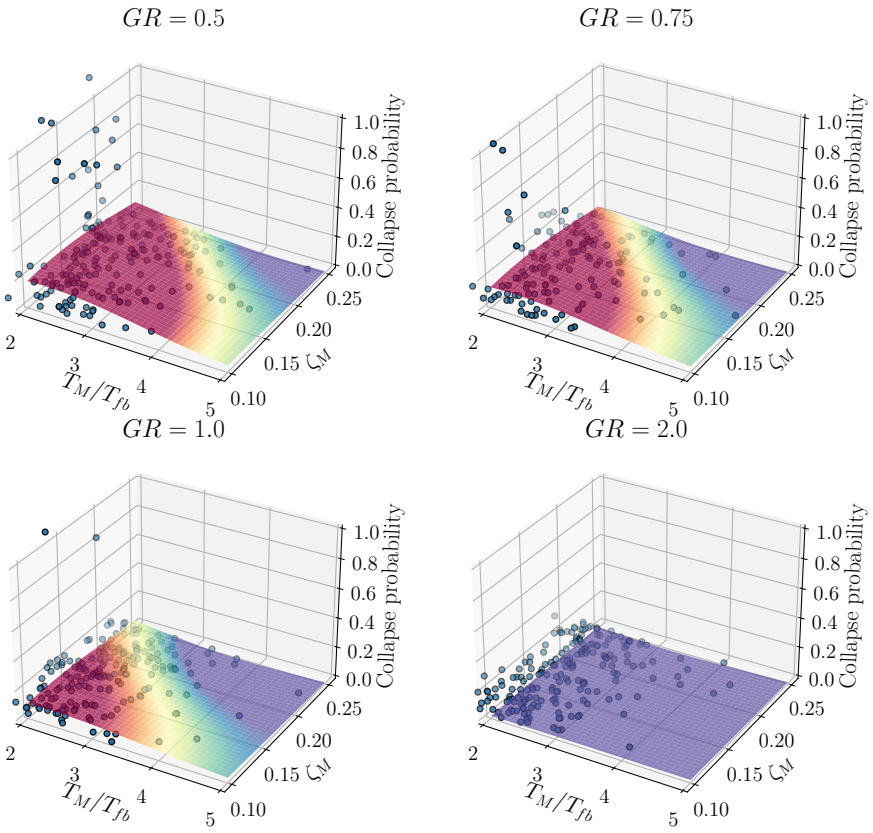

Figure 8: Effect of T_M/T_{fb} and ζ_M on GP collapse probability predictions

Increasing ζ_M does not always have a linear effect on collapse probability; the increase from $\zeta_M = 0.10$ to $\zeta_M = 0.15$ under $T_M/T_{fb} = 2.0$ results in increasing collapse probability, while further increasing ζ_M to 0.20 lowers collapse probability. Referring again to Figure 4d), the trend with ζ_M is much weaker than for the other three variables. Nevertheless, ζ_M is still a consequential variable within the GP predictions, particularly at larger T_M/T_{fb} conditions, which is a result of the selection of the isotropic squared-exponential kernel, which utilizes one shared lengthscale between all four dimensions. Although the SE-ISO kernel slightly overexaggerates the effects of a less important variable like ζ_M and vice versa, it allows for the observation of more minor trends which may be missed otherwise. As the current study is limited to collapse

probability defined on interstory drift, it is expected that T_M/T_{fb} and ζ_M might be less influential parameters compared to GR and R_y. However, they contribute to acceleration and velocity of the structure, which are important contributors to repair costs not incorporated in this study. Additionally, in design, T_M/T_{fb} and ζ_M also contribute to determining the isolator displacement capacity D_M in conjunction with GR, which has an impact on the optimization function via construction cost.

3.3. Inverse design

As an example of the inverse design process, a 4-story 4-bay frame design is sought for a design spectrum defined by $S_1 = 1.017$ g, assumed to represent the MCE_R. Using the GP output, a space of design variables that result in collapse likelihood predictions lower than a target failure probability is identified. Although the most cost optimal design is later identified and discussed, a set of Pareto optimal designs could also be presented. The set of Pareto optimal designs is obtained from the multiobjective optimization problem

$$X_{PF} = \underset{x \in X_d}{\arg\min} \{c(\mathbf{x}), p(\mathbf{x})\} \tag{15}$$

where X_{PF}, the Pareto front, is the set of design points that are dominant, meaning that no other design points simultaneously improve both the cost and the predicted collapse probability of the structure. Points not belonging to the Pareto front are considered "dominated" points. Figure 9a) shows that a large portion of the Pareto front lies in the realm of designs that achieve extremely low probabilities of collapse, which indicates that many designs are likely to achieve the 10% collapse probability target under the defined collapse definition for SMRFs. Since no truncation is used in the GP output, collapse prediction values < 0 are present and effectively represent negligible collapse probability. Figures 9b) and c) present the set of Pareto efficient designs in the space of the original design parameters. In Figure 9b), two types of designs are present: designs that minimize collapse probability with higher superstructure strength and GR values above 1.0 are clustered at the bottom of the plot, while designs at the top, with weaker structures and smaller GR, are Pareto efficient by achieving lower costs. Other than a few exceptions, designs with $\zeta_M = 0.25$ tend to be Pareto efficient (see Figure 9c) since high damping is associated with lower collapse probability while also decreasing land cost through reducing the design isolator displacement D_M; as such, Pareto efficient designs exhibit high damping. Similarly, the Pareto efficient designs span the range of T_M/T_{fb}, which shows that these designs are Pareto efficient

in reducing collapse probability (achieving the lowest collapse probability among other designs with the same cost), while the small cluster of low ζ_M and T_M/T_{fb} designs are Pareto efficient in the upfront cost dimension.

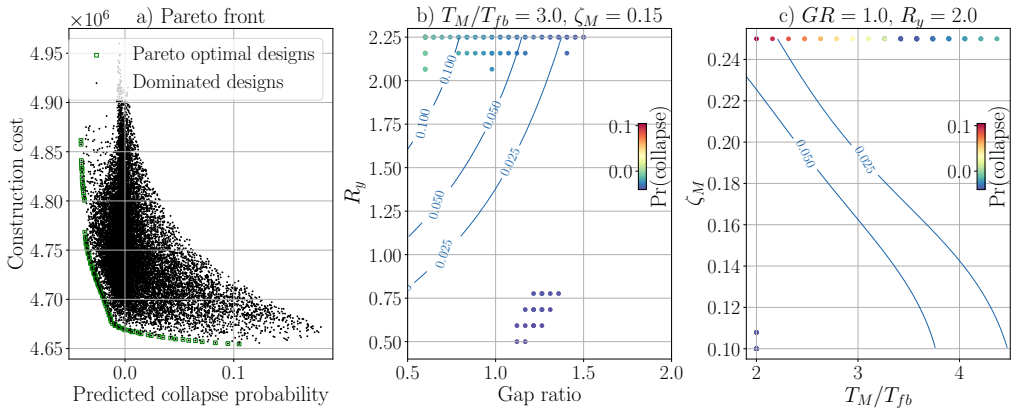

Figure 9: Illustration of Pareto efficient designs in the decision variable space

A single design is then selected from the Pareto set, optimizing the lowest upfront cost within the acceptable design space. For target collapse probabilities of 10%, 5%, and 2.5%, the design parameters are presented in Table 2. Upon optimizing for collapse probability and cost, the inverse procedure selects the minimum considered gap for all targets while increasing the isolation period T_M/T_{fb} for lower collapse targets. For a 10% collapse probability at the MCE_R level targeted by ASCE 7-22, the cost optimization aided by GP selects a design with the minimum acceptable gap of 60.0% of the code recommended displacement capacity while lowering the superstructure strength from the code recommendation to a reduction factor of $R_y = 2.25$, with an isolation ratio of $T_M/T_{fb} = 2.16$ and damping of $\zeta_M = 0.25$. It should be noted that these values lie on the boundary of the considered design space which is an artifact of a single cost metric in the optimization function. Under the current collapse definitions, the superstructure has adequate strength to avoid collapse-inducing drift ratios, though this may not be true for other superstructures such as intermediate moment frames.

For special moment frames, all three designs show parameters that have smaller moat gaps and weaker superstructure strength when compared to code minimum. These designs are consequences of (1) the collapse definition, and (2) the cost function selected. As such, they should not be taken as recommended designs. Furthermore, this study does not predict damage prior to col-

Table 2: GP inverse designed structure parameters based on cost optimization

Target % collapse	GR	T_M/T_{fb}	ζ_M	R_y	D_M	GP % collapse	Total cost
10 %	0.6*	2.16	0.25*	2.25*	18.92 cm	9.45%	\$4.655 M
5 %	0.6*	2.79	0.25*	2.25*	24.46 cm	4.64%	\$4.659 M
2.5 %	0.6*	3.10	0.25*	2.25*	27.23 cm	2.42%	\$4.663 M
Baseline	1.0	3.00	0.15	2.00	51.97 cm	5.85%	\$4.721 M

* Indicates variable lies on the bounds of the considered design space.

lapse. Functionality-focused design that aims at more stringent performance targets would result in isolation parameters that reduce story drift significantly, likely through increasing GR to minimize moat wall impact and lowering R_y to reduce overall drifts. Also not considered are damage to nonstructural components, which are often sensitive to floor accelerations and velocities and could result in the inverse design giving more weight to T_M/T_{fb} or ζ_M.

3.4. Sensitivity analysis

The optimization problem in Equation 12 is sensitive to cost definitions as well as the collapse fragility as defined in Figure 2. Figure 10 shows the change in the cost optimal design variables as several conditions are changed, including the mean drift of the collapse fragility θ, unit land cost, and unit steel cost. Changes in design variable are shown relative to the selected designs in Table 2. The collapse definition has a significant effect on the selected design. At limit states with lower θ, the necessary GR increases and R_y decreases. Thus, if designing an intermediate or ordinary moment frame with reduced ductility capacity, larger moat gaps and superstructure design strength would be required to achieve the same collapse probability. Changing the drift limit state could also be used as a proxy for conducting inverse design to achieve stricter limit states such as immediate occupancy or functionality.

The optimal inverse design also changes considerably as project constraints like resource prices change. As land and steel prices rise, there is a tradeoff to maintain the same allowable probability while minimizing cost. As land price rises, isolator displacement is reduced by lowering T_M/T_{fb}, which results in a stiffer isolator system. In response, superstructure strength is increased with the goal of keeping story drifts low. The inverse is true when steel price rises, with R_y increasing to lower the steel cost while T_M/T_{fb} increases to provide a more flexible isolation system. Figure 10d) also presents the effect of the collapse fragility definition on predicted

Table 3: Bearing and frame parameters from GP-aided inverse designs

	Design specifications							Collapse %
Target	GR	μ_1	μ_2	R_1	R_2	Largest beam	Columns	Estimated % collapse
10%	0.60	0.024	0.25	274 mm	1469 mm	W30X90	W14X257	9.45%
5%	0.60	0.057	0.11	274 mm	1469 mm	W27X84	W14X233	4.64%
2.5%	0.60	0.045	0.10	274 mm	1827 mm	W24X84	W14X233	2.42%
Baseline	1.000	0.037	0.13	764 mm	1424 mm	W27X84	W14X233	5.85%

collapse probability of the code-minimum baseline design, defined as a structure with $GR = 1.0$, $R_y = 2.0$, $T_M/T_{fb} = 3.0$, and $\zeta_M = 0.15$ that would be typical in design practice. While this study sets median collapse drift ratio θ at 0.078, the GP prediction approaches 10% as θ shifts lower to values more likely seen in intermediate moment frames, which agrees more with previous findings for isolated special moment frames, such as Masroor and Mosqueda [8], which concluded that a code-recommended design ($GR = 1.0$, $T_M/T_{fb} \simeq 2.0$, $\zeta_M \simeq 0.15$) achieved the 10% target with 9.7% collapse when defining $\theta = 0.05$.

3.5. Validation via incremental dynamic analysis

To validate the Gaussian process model results, collapse fragility curves are generated using the FEMA P-695 methodology [29] for the three designs targeting the different probabilities of collapse shown in Table 2. For a randomly selected MCE_R spectrum with $S_1 = 1.017$ g, the superstructure and isolator design parameters for the three designs are presented in Table 3. To calculate the bearing period T_M, the fixed base period is estimated from ASCE-7 procedures

$$T_{fb} = 1.4 \times 0.0724 \times h_n^{0.8} \tag{16}$$

where h_n is the height of the four-story building in meters. The inversely designed T_M/T_{fb} value is then used to calculate the bearing period T_M.

The designs are subjected to a full nonlinear IDA. Additionally, analysis is performed for a baseline design using the code-prescribed minimum displacement capacity and $R_y = 2.0$ with $T_M/T_{fb} = 3.0$ s and $\zeta_M = 0.15$ designed using the equivalent lateral force procedure in ASCE 7-22. From the library of 133 ground motions, 50 records are scaled to match the design spectrum

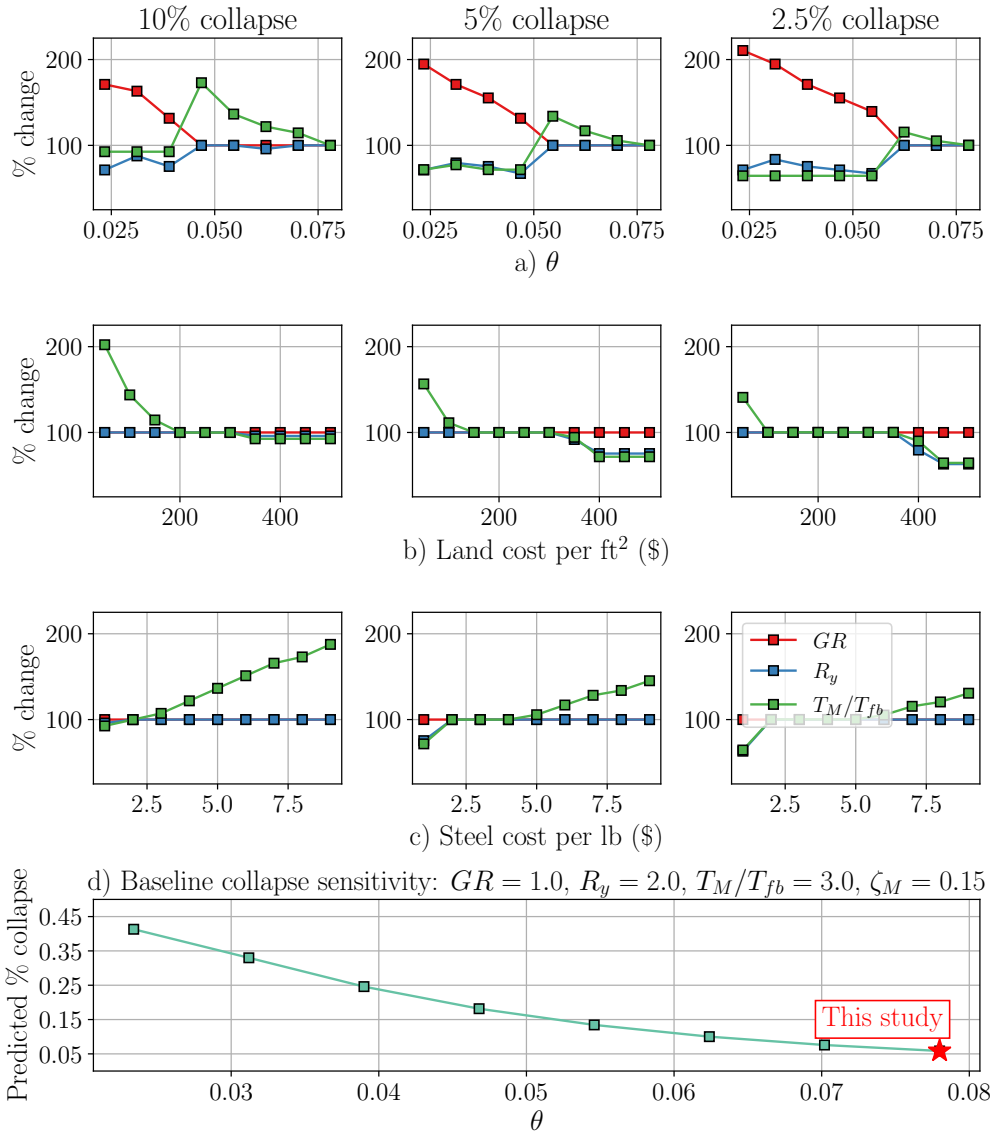

Figure 10: Sensitivity analysis for cost optimal design parameters to achieve different collapse targets across a) defined mean collapse drift, b) land cost, and c) steel cost; d) Sensitivity of predicted baseline collapse to defined mean collapse drift

amplified by 1.0×, 1.5×, and 2.0× the MCE$_R$. Figure 11 shows a boxplot of the MCE$_R$ level peak story drift of the three designs along with the baseline design as found from the nonlinear time history analyses of the ground motion suite. The boxplot shows that the median drifts

exhibit trends as expected, with lower collapse target designs experiencing less story drift than higher targets counterpart. The probability of collapse is then evaluated from drift as was done for the database generation, and the mean probability of collapse across all ground motions in the intensity level is used as a data point. A lognormal distribution is fit through the data via a maximum likelihood estimation (MLE).

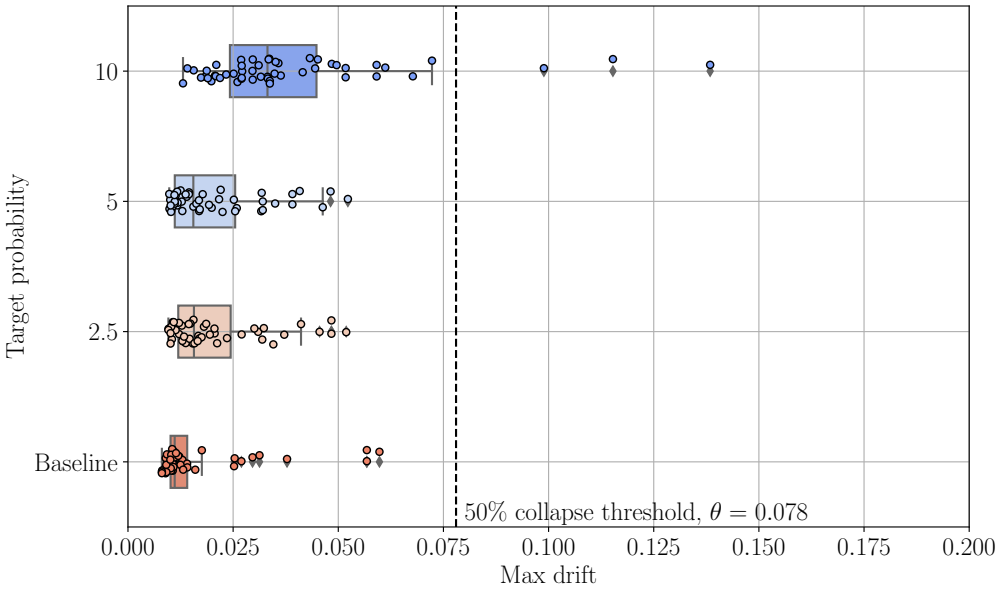

Figure 11: Boxplot of peak story drift at MCE_R level for inverse designs

Figure 12 and Table 4 present the fragility curves for the IDA performed on the inversely designed buildings. Under raw observed percentage of collapse at the MCE_R level, the 5% and 2.5% designs achieved their targeted collapse probability (1.37% and 1.53%, respectively), while the 10% design observed a collapse frequency of 11.6%. Notably, the SMRF baseline design achieved risks well below the target 10% from ASCE 7-22 with a 1.9% collapse probability at the MCE_R level, which becomes 1.6% when adjusted for the MLE fit that considers the 1.5× and 2.0× MCE levels. With the MLE fit, the GP-aided designs for 5% and 2.5% collapse met their targets with 1.73% and 1.69%, while the 10% design exceeded its target with 12.8%. Although the 5% design individually recorded lower collapse estimation at the three discrete MCE experiments than the 2.5% design, its MLE fit collapse probability at MCE = 1.0 is higher than the 2.5%. This is an artifact of the MLE curve fitting, which minimizes error among the three

points by changing the lognormal mean and dispersion parameters. Although these estimates could be adjusted for additional uncertainty through provisions in FEMA P-695 [29], likely resulting in increased collapse probabilities, this is not performed for this study since FEMA P-695 procedures were derived for fixed base structures.

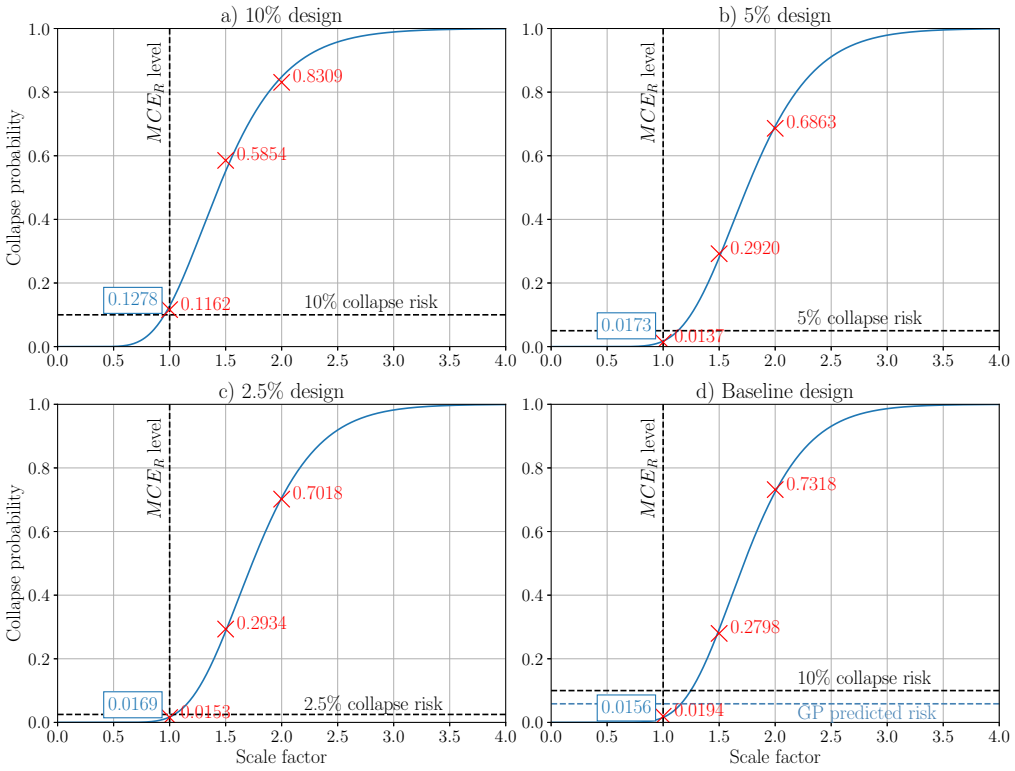

Figure 12: Collapse fragility curves of MCE_R levels from incremental dynamic analysis results for GP-aided designs

Although not all GP-aided designs achieved their intended collapse probability, the GP-aided inverse design method gives an initial estimate for the magnitude of displacement capacity, isolation period amplification, and strength requirements necessary to target lower collapse probabilities. The validation study highlights the difficulty of predicting collapse with consistent accuracy at all performance targets. Although the 2.5% design performed close to its target, the 10% and 5% achieved true collapse probabilities that were 2.78% and 3.27% away from their targets, respectively. Notably, the baseline special moment resisting frame, as modeled in this study, performs extremely well under the defined collapse definition. Without considering

Table 4: Incremental dynamic analysis results for GP-aided designs

	Observed collapse frequency			Lognormal MLE fit collapse frequency at MCE_R level	Lognormal parameters
Target	1.0 MCE	1.5 MCE	2.0 MCE	Fit value (GP prediction)	Mean (dispersion, β)
10%	11.6%	58.5%	83.1%	12.8% (9.45%)	1.44 (0.320)
5%	1.37%	29.2%	68.6%	1.73% (4.64%)	1.75 (0.265)
2.5%	1.53%	29.3%	70.2%	1.69% (2.42%)	1.74 (0.260)
Baseline	1.93%	28.0%	73.2%	1.56% (5.85%)	1.72 (0.252)

additional functionality objectives, the GP-aided inverse design procedure offers a design that achieves closer to the intended 10% probability of collapse.

4. Conclusions

To evaluate how isolated buildings might be designed to achieve targeted collapse probabilities under a given earthquake level, such as the targets given in ASCE-7 [4], a GP model was developed to identify acceptable design spaces over which the design can be optimized. For an SMRF, the moat gap distance, superstructure strength, and isolation ratio are the most important variables for controlling the collapse probability, in that order. An increase in these variables results in a larger decrease in predicted collapse probability compared to changing the isolation system damping. The GP model predicts that to achieve the ASCE-7 target of 10% probability of collapse for an isolated SMRF with $R_y = 2.0$, $T_M/T_{fb} = 3.0$, $\zeta_M = 0.15$, the moat gap needs only to be 0.93 times the current code minimum. This gap recommendation can be lowered to 0.47 if R_y is lowered to 1.5. The gap ratio for the same isolated SMRF should increase to 27% and 50% greater than code recommended minimum when targeting 5% and 2.5% collapse probability, respectively. These conclusions are only for collapse of special moment frames and do not extend to any other level of functionality, such as immediate occupancy or repairable damage or any other superstructure type such as intermediate moment frames, braced frames, etc.

From the acceptable design region, optimization can be used to select a final design. This study optimized using upfront steel and land cost. Throughout the inverse design procedure, to lower collapse probabilities, GP-aided design increased the ratio between the isolator and fixed base superstructure to further concentrate deformations into the isolation layer. Interestingly,

the gap ratio was maintained. Under the collapse fragility definitions used in this study, special moment frames are predicted to have adequate ductility to withstand high forces from wall impact and prevent collapse. Sensitivity analysis shows that GP prediction is able to change design strategy depending on project constraints, such as resource prices or drift fragility definitions.

Validation results showed that current minimum code design recommendations achieve a collapse probability well below 10% at the MCE_R level for isolated SMRFs. Sensitivity analysis of the GP shows that changing the collapse fragility definition to have drift fragility curve definitions resembling intermediate moment frames results in predicted collapse rising closer to the intended 10% as laid out in ASCE 7. For the 10% collapse probability target, the inverse design using GP predictions suggested that the gap can be 0.60 times the code displacement capacity in combination with a strength reduction factor of $R_y = 2.25$, $T_M = 2.16T_{fb}$ s, and $\zeta_M = 0.25$, which was validated to achieve 12.8% collapse, thus being closer to, albeit exceeding, the intended 10% collapse target. For all design targets, GP-aided designs achieved collapse probabilities close to their targeted performance. Discrepancies between the GP predictions and validation results highlight the difficulty in predicting collapse probability at enhanced targets due to high uncertainty. For future work, the usage of a non-homogeneous variance parameter in the GP kernel could serve to provide lowered uncertainty in certain regions of the design domain, leading to predictions with a standard deviation bound. The findings of the inverse design framework could also be further developed by considering full 3D models as well as both horizontal direction and vertical shaking. Overall, the usage of GP modeling on a database of generalized parameters allows for the interaction between all variables and their effects on collapse probability to be better observed and different levels of performance to be targeted. The variables and methods presented are well suited to be extended to more general design problems beyond a handful of design case studies.

Data availability

All datasets and computational scripts that support the findings of this study are available from the NSF NHERI DesignSafe Data Depot: PRJ-4797 .

Funding sources

Funding: This work was supported by the National Science Foundation Graduate Research Fellowship [grant numbers DGE 2146752 , DGE 1752814].

References

[1] T. A. Morgan, S. A. Mahin, Achieving reliable seismic performance enhancement using multi-stage friction pendulum isolators, Earthquake Engineering & Structural Dynamics 39 (13) (2010) 1443–1461. doi:10.1002/eqe.1043.

[2] S. Moretti, A. Trozzo, V. Terzic, G. P. Cimellaro, S. Mahin, Utilizing base-isolation systems to increase earthquake resiliency of healthcare and school buildings, Procedia Economics and Finance 18 (2014) 969–976. doi:10.1016/S2212-5671(14)01024-7.

[3] V. Terzic, S. Mahin, M. Comerio, Comparative life-cycle cost and performance analysis of structural systems for buildings, in: Tenth US National Conference on Earthquake Engineering, 2014.

[4] ASCE 7-22, Minimum Design Loads and Associated Criteria for Buildings and Other Structures, 1st Edition, Vol. v.ASCE/SEI 7-22, American Society of Civil Engineers, Reston, 2021. doi:10.1061/9780784414248.

[5] Y. Bao, T. C. Becker, Effect of design methodology on collapse of friction pendulum isolated moment-resisting and concentrically braced frames, Journal of Structural Engineering 144 (11) (2018) 04018203. doi:10.1061/(ASCE)ST.1943-541X.0002183.

[6] B. Shao, S. A. Mahin, A probabilistic design method to achieve targeted levels of reliability for seismically isolated structures, Earthquake Spectra 36 (2) (2020) 741–766. doi:10.1177/8755293019891728.

[7] S. Kitayama, M. C. Constantinou, Collapse performance of seismically isolated buildings designed by the procedures of ASCE/SEI 7, Engineering Structures 164 (2018) 243–258. doi:10.1016/j.engstruct.2018.03.008.

[8] A. Masroor, G. Mosqueda, Assessing the collapse probability of base-isolated buildings considering pounding to moat walls using the FEMA P-695 methodology, Earthquake Spectra 31 (4) (2015) 2069–2086. doi:10.1193/092113EQS256M.

[9] C. Ning, Y. Xie, Risk-based optimal design of seismic protective devices for a multicomponent bridge system using parameterized annual repair cost ratio, Journal of Structural Engineering 148 (5) (2022) 04022044. doi:10.1061/(ASCE)ST.1943-541X.0003330.

[10] I. Gidaris, A. A. Taflanidis, G. P. Mavroeidis, Kriging metamodeling in seismic risk assessment based on stochastic ground motion models, Earthquake Engineering & Structural Dynamics 44 (14) (2015) 2377–2399. doi:10.1002/eqe.2586.

[11] I. Gidaris, A. A. Taflanidis, G. P. Mavroeidis, Multiobjective design of supplemental seismic protective devices utilizing lifecycle performance criteria, Journal of Structural Engineering 144 (3) (2018) 04017225. doi:10.1061/(ASCE)ST.1943-541X.0001969.

[12] I. Gidaris, A. A. Taflanidis, D. Lopez-Garcia, G. P. Mavroeidis, Multi-objective risk-informed design of floor isolation systems, Earthquake Engineering & Structural Dynamics 45 (8) (2016) 1293–1313. doi:10.1002/eqe.2708.

[13] S. M. Spence, Optimization of uncertain and dynamic high-rise structures for occupant comfort: An adaptive kriging approach, Structural Safety 75 (2018) 57–66. doi:10.1016/j.strusafe.2018.05.008.

[14] A. Suksuwan, S. M. Spence, Performance-based multi-hazard topology optimization of wind and seismically excited structural systems, Engineering Structures 172 (2018) 573–588. doi:10.1016/j.engstruct.2018.06.039.

[15] F. McKenna, M. H. Scott, G. L. Fenves, Nonlinear finite-element analysis software architecture using object composition, Journal of Computing in Civil Engineering 24 (1) (2010) 95–107. doi:10.1061/(ASCE)CP.1943-5487.0000002.

[16] D. M. Fenz, M. C. Constantinou, Modeling triple friction pendulum bearings for response-history analysis, Earthquake Spectra 24 (4) (2008) 1011–1028. doi:10.1193/1.298253.

[17] T. C. Becker, S. A. Mahin, Approximating peak responses in seismically isolated buildings using generalized modal analysis, Earthquake engineering & structural dynamics 42 (12) (2013) 1807–1825. doi:10.1002/eqe.2299.

[18] D. G. Lignos, H. Krawinkler, Deterioration modeling of steel components in support of collapse prediction of steel moment frames under earthquake loading, Journal of Structural Engineering-Reston 137 (11) (2011) 1291. doi:10.1061/(ASCE)ST.1943-541X.0000376.

[19] N. D. Dao, K. L. Ryan, E. Sato, T. Sasaki, Predicting the displacement of triple pendulum bearings in a full-scale shaking experiment using a three-dimensional element, Earthquake engineering & structural dynamics 42 (11) (2013) 1677–1695. doi:10.1002/eqe.2293.

[20] S. Muthukumar, R. DesRoches, A hertz contact model with non-linear damping for pounding simulation, Earthquake engineering & structural dynamics 35 (7) (2006) 811–828. doi:10.1002/eqe.557.

[21] S.-Y. Yun, R. O. Hamburger, C. A. Cornell, D. A. Foutch, Seismic performance evaluation for steel moment frames, Journal of Structural Engineering 128 (4) (2002) 534–545. doi:10.1061/(ASCE)0733-9445(2002)128:4(534).

[22] T. D. Ancheta, R. B. Darragh, J. P. Stewart, E. Seyhan, W. J. Silva, B. S.-J. Chiou, K. E. Wooddell, R. W. Graves, A. R. Kottke, D. M. Boore, et al., NGA-West2 database, Earthquake Spectra 30 (3) (2014) 989–1005. doi:10.1193/070913EQS197M.

[23] C. K. Williams, C. E. Rasmussen, Gaussian processes for machine learning, Vol. 2, MIT press Cambridge, MA, 2006. doi:10.7551/mitpress/3206.001.0001.

[24] J. Nocedal, Quasi-Newton Methods, 2nd Edition, Springer,, New York :, 2006. doi:10.1007/978-0-387-40065-5_6.

[25] J. Sacks, S. B. Schiller, W. J. Welch, Designs for computer experiments, Technometrics 31 (1) (1989) 41–47. doi:10.1080/00401706.1989.10488474.

[26] A. P. Kyprioti, J. Zhang, A. A. Taflanidis, Adaptive design of experiments for global kriging metamodeling through cross-validation information, Structural and Multidisciplinary Optimization 62 (3) (2020) 1135–1157. doi:10.1007/s00158-020-02543-1.

[27] S. Sundararajan, S. Keerthi, Predictive approaches for choosing hyperparameters in gaussian processes, Advances in neural information processing systems 12 (1999).

[28] S. Kitayama, H. Cilsalar, Seismic loss assessment of seismically isolated buildings designed by the procedures of ASCE/SEI 7-16, Bulletin of Earthquake Engineering 20 (2) (2022) 1143–1168. doi:10.1007/s10518-021-01274-y.

[29] FEMA P-695, Quantification of building seismic performance factors, ATC-63 report, Federal Emergency Management Agency, 2009.